02P-155

The HCCI Combustion Process in a Single Cycle – High-Speed Fuel Tracer LIF and Chemiluminescence Imaging

Anders Hultqvist *, Magnus Christensen, Bengt Johansson
Div. of Combustion Engines, Dept. of Heat and Power Engineering, Lund Institute of Technology

Mattias Richter, Jenny Nygren, Johan Hult, Marcus Aldén
Div. of Combustion Physics, Lund Institute of Technology

*Scania CV AB

ABSTRACT

The Homogeneous Charge Compression Ignition (HCCI) combustion progress has been characterized by means of high-speed fuel tracer Planar Laser Induced Fluorescence (PLIF) combined with simultaneous chemiluminescence imaging. Imaging has been conducted using a high-speed laser and detector system. The system can acquire a sequence of eight images within less than one crank angle. The engine was run at 1200 rpm on iso-octane or ethanol and a slight amount of acetone was added as a fuel tracer, providing a marker for the unburned areas. The PLIF sequences showed that, during the first stage of combustion, a well distributed decay of fuel concentration occurs. During the later parts of the combustion process the fuel concentration images present much more structure, with distinct edges between islands of unburned fuel and products. The transition between the evenly distributed fuel oxidation in the beginning and the large structures at the end, is most likely the result of a gradual amplification of small temperature inhomogeneities and an expansion of burned gas compressing the unburned.

INTRODUCTION

In a Homogeneous Charge Compression Ignition (HCCI) engine, the fuel and air are premixed to create a homogeneous charge. During the compression stroke, the charge is heated to obtain auto-ignition close to Top Dead Center (TDC). The cycle-to-cycle variations in Indicated Mean Effective Pressure (IMEP) of the HCCI combustion process are very small [1,2] since combustion initiation occurs in many places simultaneously [3]. Since ignition occurs at multiple points, the integrated combustion rate becomes very high. Therefore, highly diluted mixtures or exhaust gas recirculation (EGR) have to be used in order to limit the rate of combustion [4]. With HCCI, there is no direct means to control the start of combustion as the ignition process relies on spontaneous auto-ignition. By adjusting the remote operating parameters e.g. inlet temperature or EGR rate, ignition timing can be controlled [5,6]. The major advantages of HCCI compared to the diesel engine are low NOx emissions and, depending on the fuel, virtually no soot [7]. The benefit of HCCI compared to the Spark Ignition (SI) engine is the much higher part load efficiency [8]. The toughest challenge is controlling the ignition timing over a wide load and speed range [9,10]. Another challenge is to obtain an acceptable power density. The power density is limited by combustion noise and high peak pressures. At low loads, the rather high emissions of unburned hydrocarbons and carbon monoxide, in combination with low exhaust temperatures, present an additional challenge [11]. By applying unthrottled HCCI combustion at part load in SI engines, efficiency can be improved by 40-100%. Emerging technologies for variable valve timing, with the intent of using these as a means of controlling the combustion timing in HCCI engines [12], may well lead the way for a dual mode SI/HCCI-engine, thus gaining the benefits of throttle-less operation and smooth running at low loads and the power density of the conventional SI engine at high loads.

The HCCI combustion process has previously been studied through different imaging techniques by Richter et al. [13,14] and other researchers [15,16,17]. The visualization of the combustion process has proven a valuable tool in understanding the combustion process. Experiments with chemiluminescence imaging [18] and planar laser induced fluorescence [19] indicate that the combustion process is delayed along the cool combustion chamber walls. However, combustion-to-wall interaction was not found to be the main mechanism responsible for the emissions of unburned hydrocarbons [19].

In previous experiments [14,19], comprising single shot PLIF measurements in HCCI engines, it was found that different types of structures appear at different points in time as the combustion progresses. From the measurements, it was impossible to decide whether or not the structures grew and if so, how fast the growth was. Furthermore, the single shot measurements did not reveal if new ignition kernels appeared during the combustion event.

In the present experiments, two truck-sized engines were used to study the HCCI combustion process with two high-speed imaging techniques, Planar Laser Induced Fluorescence (PLIF) and chemiluminescence imaging. Even though the HCCI combustion progress relies on slow chemistry, it is a chemistry that occurs simultaneously throughout the combustion chamber. This is why the over all rate of heat release is high. Using the high speed imaging system, it is possible to determine whether there is only a distributed gradual consumption of fuel or if there are reaction fronts that spread. Some simple image processing tools are used to enhance structures and to analyze gradients and histograms of the measured fuel concentrations. The result of this analysis is then compared with a known case; turbulent flame propagation in an SI engine.

EXPERIMENTAL SETUP

OPTICAL ENGINES

Two truck-sized heavy-duty engines, a Scania D12 and a Volvo TD-100, were used for this study. The Scania D12 single cylinder engine was equipped with a Bowditch type optical access to enable imaging of most of the combustion chamber. To keep the vibrations from the oscillating masses on a low level, the engine was equipped with two pairs of counter rotating balancing shafts contained in the oil sump. The engine and the dynamometer were rigidly joined with a floating framework, so as not to transfer any vibrations to the surroundings. On the intake and exhaust side, pressure equalization vessels were fitted. A piezoelectric pressure transducer was used to record the cylinder pressure. In Figure 1, the optical engine is displayed with its cylinder liner dropped down to its lower position for cleaning. The neat design, also used at IFP and Sandia National Labs., with a “drop-down” liner, provides swift access to the inner glass surfaces for cleaning or inspection. A cleaning cycle is completed within five minutes, which can be compared to a conventional head disassembly, which requires about one hour.

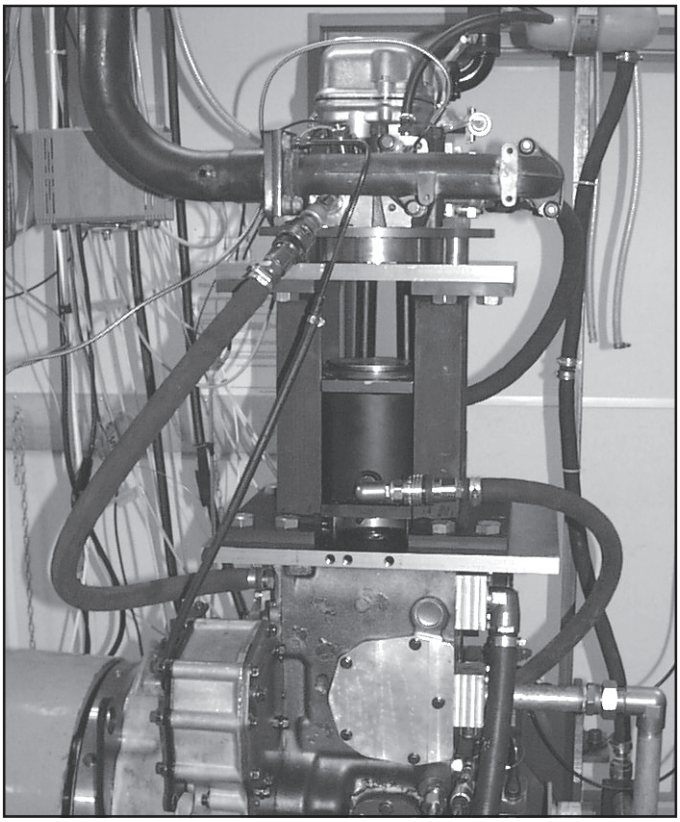

Figure 1: Photo of the Scania D12 single cylinder engine.

The compression ratio was set to 16:1 and a mixture of iso-octane/acetone or ethanol/acetone was fed to the engine using a port fuel injection system. Acetone was mixed into the base fuel to act as a fuel tracer. The fuel was injected 1.5 m upstream of the inlet, promoting good mixing and the forming of a homogenous charge. This to ensure that what is studied is the combustion process rather than the effects of the mixture formation process. In Table 1 and Table 2, the basic engine specifications are shown. In some measurements, ethanol was used as fuel instead of iso-octane since the problems with laser light absorption are then less significant. It is well known that iso-octane does not show any absorption around 266 nm. The mentioned absorption is introduced by intermediate species created during the latter part of the compression stroke and in the early phase of combustion [13].

The inlet air was preheated with an electrical heater to initiate HCCI combustion with the selected compression ratio and fuel type. In the Volvo TD-100 the imaging was done under the operating conditions shown in Table 3. The

Table 1: Scania D12 engine specifications.

Displaced Volume	1951 cm^3
Bore	127 mm
Stroke	154 mm
Connecting Rod	255 mm
Inlet Valve Seat Diameter	2x 39.7 mm
Exhaust Valve Seat Diameter	2x 38 mm
Valve Lift Exhaust	15 mm
Valve Lift Inlet	15 mm
Swirl Ratio	1.7
Compression Ratio	16:1
Combustion Chamber	Pancake

Table 2: Volvo TD-100 engine specifications.

Displaced Volume	1600 cm^3
Bore	120.65 mm
Stroke	140 mm
Connecting Rod	260 mm
Inlet Valve Diameter	50 mm
Exhaust Valve Diameter	46 mm
Valve Lift Exhaust	13.4 mm
Valve Lift Inlet	11.9 mm
Compression Ratio	10:1
Combustion Chamber	Pancake

Table 3: Operating conditions for the Volvo TD-100.

Inlet Temperature	100-180 °C
Inlet Pressure	1 bar (a)
Engine Speed	1200 rpm
Fuel	75% n-heptane
Tracer	25% acetone
Lambda	2.9-4

Table 4: Operating conditions for the Scania D12.

Inlet Temperature	100-180 °C
Inlet Pressure	1 bar (a)
Engine Speed	1200 rpm
Fuel	90% iso-octane or 90 % ethanol
Tracer	10% acetone
Lambda	3.8-4.2

relatively low compression ratio (10:1) of this engine called for the use a fuel with low octane rating such as n-heptane. For the Volvo TD-100, relative air/fuel-ratio lambda was varied from 2.9 to 4 in order to reveal the effect of engine load on the combustion process. For the Scania D12 engine, lambda was kept at approximately 4, see Table 4. All measurements were conducted on cool engines while progressively heating up and consequently, the inlet air temperature had to be governed to maintain proper combustion timing.

OPTICAL ACCESS

An optical engine design of the Bowditch type was chosen for the Scania D12 engine since it provides optical access to a large part of the combustion chamber. The design allows 75% of the bore to be imaged. Another advantage is the ability of three-way optical access, which is crucial for laser diagnostics. Another, more simple, design was utilized in the Volvo TD-100 engine. This design is comprised of an extended piston and a spacer fitted with four quartz windows between the engine block and the cylinder head. The Volvo TD-100 engine is shown in Figure 2. A sectioned view of the Scania D12 engine is shown in Figure 3.

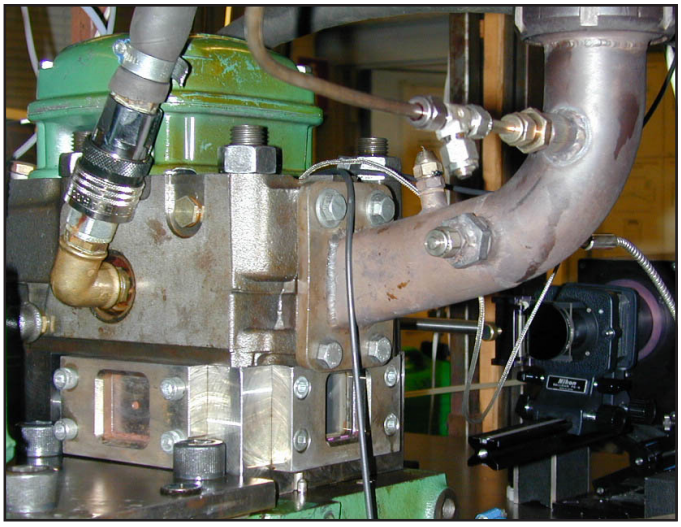

Figure 2: Photo of the Volvo TD-100 engine, fitted with a spacer providing the optical access.

In Figure 4, the optical engine is displayed from the exhaust side, fully assembled and ready to run. The piston is positioned in TDC in the figure and the piston crown can barely just be seen through the quartz ring. Also visible in the figure is the skewed view through the piston extension and the piston crown, and it is possible to catch a glimpse of one of the exhaust valves.

LASER AND DETECTOR SYSTEM

The HCCI concept features a very rapid combustion. In order to capture LIF images from the combustion event within one single cycle, it is necessary to have a high-speed imaging system. The laser system used in the presented investigations consists of four individual, high power, Nd:YAG-lasers (BMI/CSF-Thomson) [25]. Each laser in the cluster has a Q-switched oscillator and a single stage amplifier. The four laser beams are combined into one single output beam using a patented beam combining system. In this process the beams are also frequency doubled from 1064 nm to 532 nm. For excitation of the fuel tracer, an additional fourth harmonic crystal was mounted

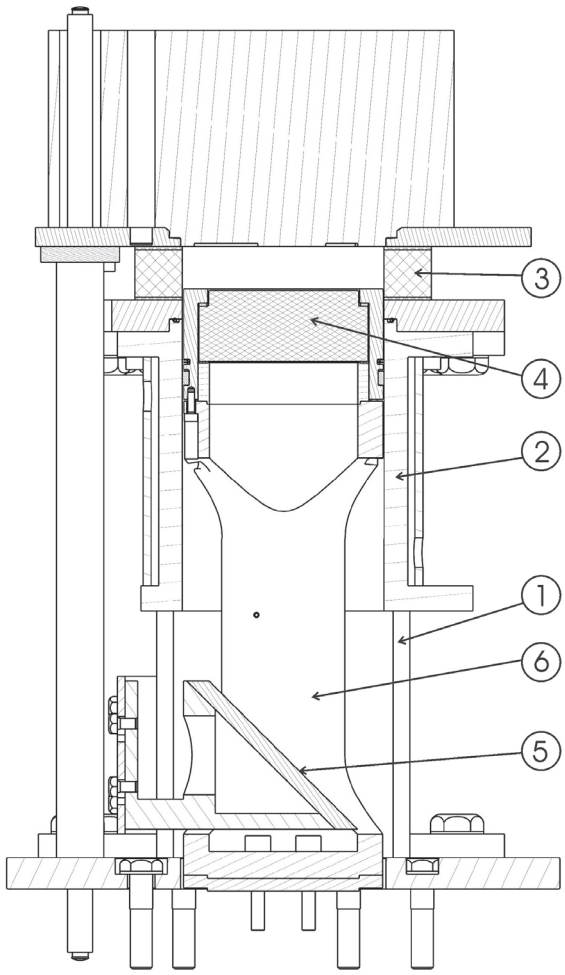

Figure 3: A sectioned view of the Scania D12 engine; (1) U-beams, (2) cylinder liner, (3) quartz ring, (4) quartz glass piston-crown, (5) mirror, (6) piston extension.

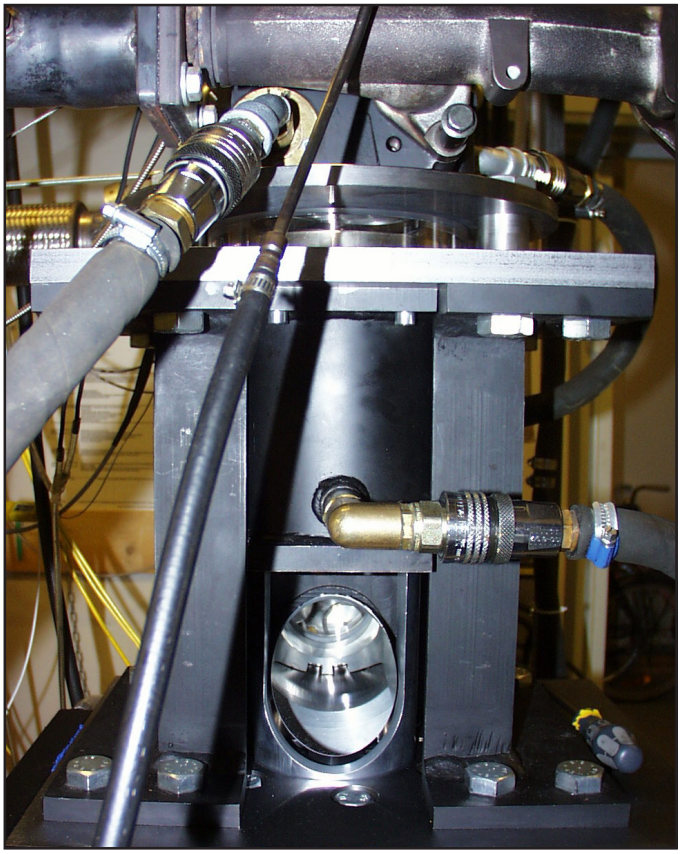

Figure 4: The Bowditch type Scania D12 engine, ready to run.

after the beam combining system, giving an output wavelength of 266 nm.
Each laser unit can be run in double pulse mode, providing a total output of eight pulses. The overall repetition rate of the system is 10 Hz. However, by firing the four lasers in series, with an arbitrary delay between the shots, a rapid burst of up to eight pulses can be achieved. If only four pulses are needed, the time delay can be set to any value between 0 and 100 ms. When the system is run in double pulse mode the time separation between two pulses from one laser is limited to 25-145 µs. These limits are governed by the length of the flash-lamp pump-pulse and the gain build-up time in the Nd:YAG oscillators. To achieve a shorter spacing the pulse-pairs from the four lasers can be overlapped in time. Thus the lower limit can be reduced to 6.25 µs (25 µs/4) when equidistant pulses are desired.
In single pulse operation, the maximum pulse energy is approximately 500 mJ/pulse at 532 nm. In double pulse mode, pulse energies are highly dependent on the time separations between pulses from individual lasers, with a maximum reading of approximately 200 mJ/pulse, occurring at a separation of 80 µs.
To match the rapid pulse burst from the laser system, a modified framing camera (Imacon 468, DRS Hadland) was used for signal detection. The camera unit consists of eight independent CCD cameras mounted in a cluster. Each CCD (576x385 pixels, 8-bit resolution) is equipped with a gateable image intensifier. An 8-facet Casegrainian beam splitter relays the image from a single optical input to the eight CCD detectors. Hence, the incoming light is split and relayed to all camera units simultaneously. By gating the image intensifiers individually, a rapid sequence of eight images can be recorded. The minimum time separation between consecutive images is 10 ns, corresponding to a frame rate of 100 MHz.
The image splitting optics are not UV transparent. In order to increase the sensitivity of the system and to detect signals in the UV spectral region, an additional image intensifier can be mounted at the entrance port. Even though sub-microsecond decay phosphors have been used in this intensifier, it reduces the maximum frame rate to 1 MHz. However, at 1200 rpm this corresponds to 138 images/cad.

OPTICAL SETUP

For the measurements in the Scania D12 engine, the laser beam from the Nd:YAG laser cluster was formed into a horizontal sheet by using a combination of a negative cylindrical lens (f=-75 mm) and a spherical lens (f=+500 mm), see Figure 5. The dimensions of the laser sheet, which was positioned in the center of the quartz cylinder liner, were 50x0.4 mm^2. The energy per pulse was approximately 30 mJ at 266 nm, and had a pulse separation of 69 µs (1/2 CAD). The fluorescence signal was detected through the piston window using an achromatic quartz lens (f=100 mm, f#=2). In front of the lens two filters were used. The first filter was a long-pass filter (λ>335 nm), which transmitted the LIF signal and rejected scattered laser light at 266 nm. The second filter was a short-pass filter (λ<470 nm), which transmitted the LIF signal and rejected fluorescence from oil residues at the cylinder surfaces and windows.
For the corresponding measurements in the TD-100

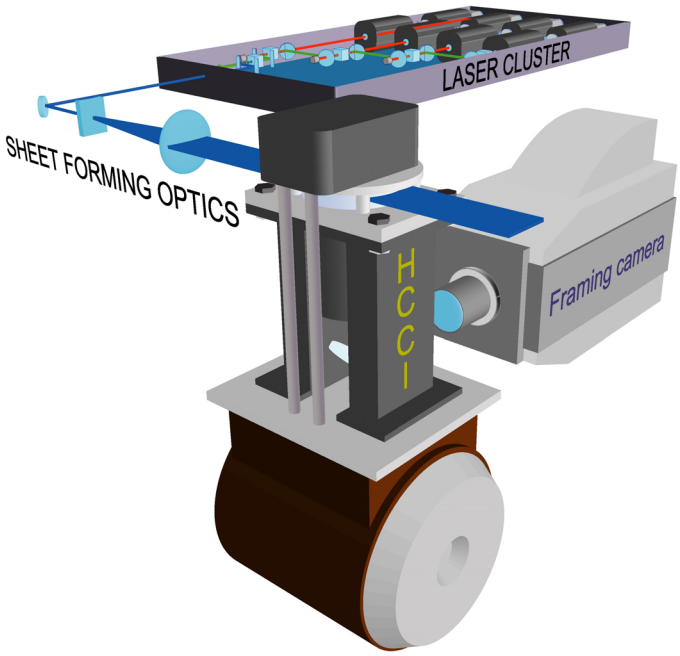

Figure 5: Optical setup for measurements in the Scania D12 engine.

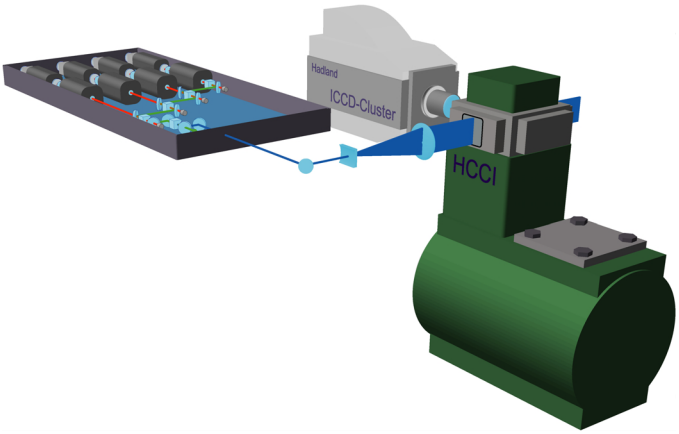

Figure 6: Optical setup for measurements in the Volvo TD-100 engine.

engine, the laser sheet was oriented vertically through the combustion chamber. The fluorescence was detected through a perpendicular side window as illustrated in Figure 6. The laser sheet size was 20x0.4 mm^2.

FUEL TRACER PLIF

Planar Laser Induced Fluorescence, PLIF, with an excitation wavelength of 266 nm, was used for the fuel visualization measurements. The fuels used were either isooctane or ethanol. As neither of these fuels show any fluorescence by themselves, it is necessary to add a fluorescent tracer species. In this work acetone was chosen as fluorescent tracer to the fuels. A concentration of 10% acetone was added to the fuels during the measurements, acting as a marker for the unburned regions. An exception to this was the measurements performed in the low compression TD100 engine where a blend of 25% aceton in 75% n-heptane was used.
Recent work has focused on finding suitable tracers to be added to a reference fuel. A suitable tracer should have the appropriate characteristics: The fluorescence should be spectrally well separated from the region of absorption. The intensity of the fluorescence signal should be independent of temperature, pressure and the composition of the surrounding gas. The tracer must follow the fuel and be consumed during combustion to avoid tracer build-up. Another important characteristic that is required is that the tracer does not influence the combustion process itself.
Pyrolysis of acetone, temperature dependence of the fluorescence yield and trapping are other potential sources of errors. Experiments performed by Yip et al. [20] showed that there is no significant pyrolysis of acetone below 1000K. In the presented experiments, the acetone LIF signal survives the cool-flame. Furthermore the detected start of consumption of acetone matches well with the start of the main heat release calculated from the pressure trace. This implies that measurements during the hotter part (1200-1400 K) of the main heat release may actually measure acetone pyrolysis. Pyrolysis is of course one step towards eventually oxidizing the fuel, and thus no error can be attributed to this behavior. As mentioned earlier, the fuel was injected 1.5 meter upstream of the inlet port. In combination with the preheated air this strategy provides a completely homogeneous mixture in the combustion chamber [14]. Hence, the difference in boiling temperature between acetone and the fuels used is not an important issue in these experiments.
Generally, the fluorescence yield of acetone shows a temperature dependence. Depending on the excitation wavelength, the yield can increase or decrease with increasing temperature. In these experiments, employing excitation at 266 nm, the sensitivity to temperature change is fair [21,22,26]. Trapping is not believed to be a problem since the absorption peak is located far away from the peak of the fluorescence emission spectra, which is in the wavelength region between 350 and 550 nm, with a maximum occurring around 420 nm.

IMAGE PROCESSING

The PLIF images exhibit problems with absorption along the path of the laser sheet and lasers having different profiles. To compensate for this, a number of image processing steps have been applied to the raw images (S) before they are analyzed and presented (I):

$$I=(S-B)/(P*A) \quad (1)$$

First, a background (B) is subtracted after which compensations for laser intensity profile inhomogeneities and laser sheet absorption are made. The mean laser profile (P) for each of the laser pulses is extracted from unburned regions in a mean LIF image averaged over 25 cycles. The individual images of a sequence are then divided by the corresponding laser profile. However, this does not compensate for small shot-to-shot variations in laser profile and laser energy or long term drift. From unburned regions in the averaged LIF images, the absorption along the path of the laser sheet can be determined. The individual images are then divided by the extracted mean absorption curve (A).
For some sequences, the corresponding gradient fields have been calculated using the Sobel transform [24] on low pass filtered images. The low pass filtering is necessary to reduce the influence of noise on the gradient calculation.

RESULTS

Cycle resolved sequences are presented to show that the HCCI combustion process is propagating in space as well as consuming fuel gradually. First, a number of fuel tracer PLIF sequences are presented. This is followed by a more detailed analysis in which histograms of the fuel distribution and gradients of the fuel distribution in the HCCI combustion process are presented. They are also compared with those of a spark ignition process. The progress of the combustion structures is illustrated by thresholded sequences. From these sequences, the burned area expansion rate is estimated. Simultaneous PLIF and chemiluminescence sequences are presented to show the correlation between combustion and fuel tracer. Finally, the effects of a varying air/fuel ratio are investigated.

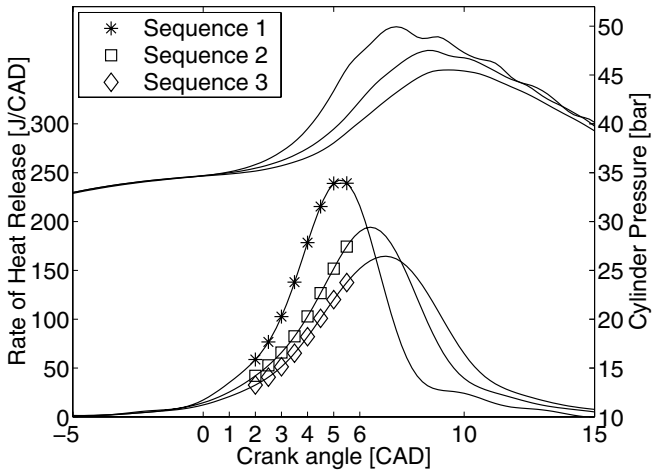

Figure 7: Pressure trace and rate of heat release, no: 1-3.

COMBUSTION PROGRESS

The pressure traces and fuel PLIF images from three sequences recorded under identical conditions in the HCCI engine are shown in Figure 7 and in Figure 8 respectively. In the beginning of the combustion process, fuel consumption starts in a number of regions in the cylinder, where small inhomogeneities in temperature or fuel mixture are favorable to reactions. Initially the fuel is gradually consumed by local reactions in these regions, and the fuel consumption process is completely different from that of a propagating flame which is the case e.g. in an SI engine.

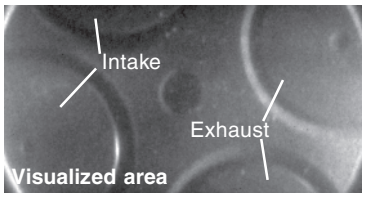

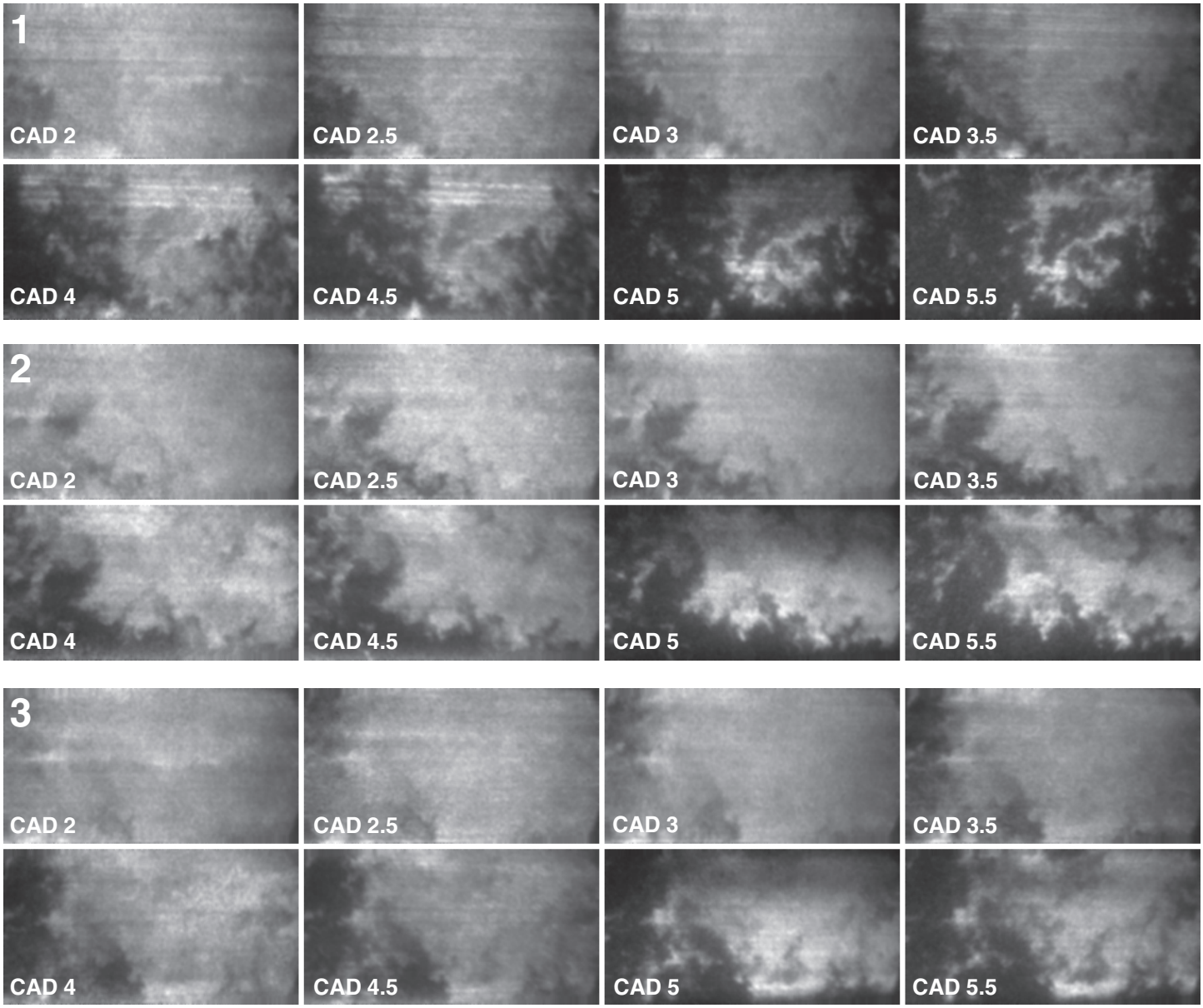

Figure 8: Fuel tracer PLIF sequences no: 1-3, corresponding to three different cycles, recorded under identical conditions in the Scania D12 HCCI engine. The imaged region corresponds to 95x50 mm^2, the time separation between images is 69 µs. (69 µs corresponds to 1/2 CAD at 1200 rpm)

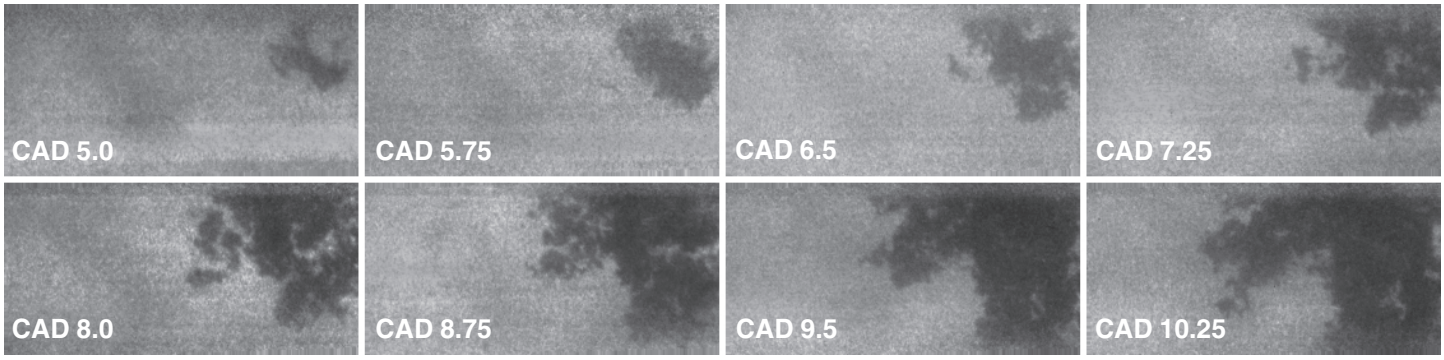

Figure 9: Fuel tracer PLIF sequence recorded in an SI engine, the imaged region corresponds to 50x25 mm².

There are no sharp borders between burnt and unburned gases, and the fuel concentration gradually decreases during the cycle, with little or no expansion of the reaction region. During the entire combustion event, new ignition kernels appear at locations that have become favorable because of the global pressure rise.

For comparison, a fuel PLIF sequence recorded in an SI engine is shown in Figure 9. It was recorded in a small single cylinder, four-stroke, side-valve SI engine [23]. In the SI engine combustion takes place with a highly turbulent flame propagation. The gradient between burned and unburned zones is very sharp. An additional visual difference between a propagating turbulent flame in an SI engine and HCCI combustion is the large number of separated flame islands, caused by the multiple ignition kernels.

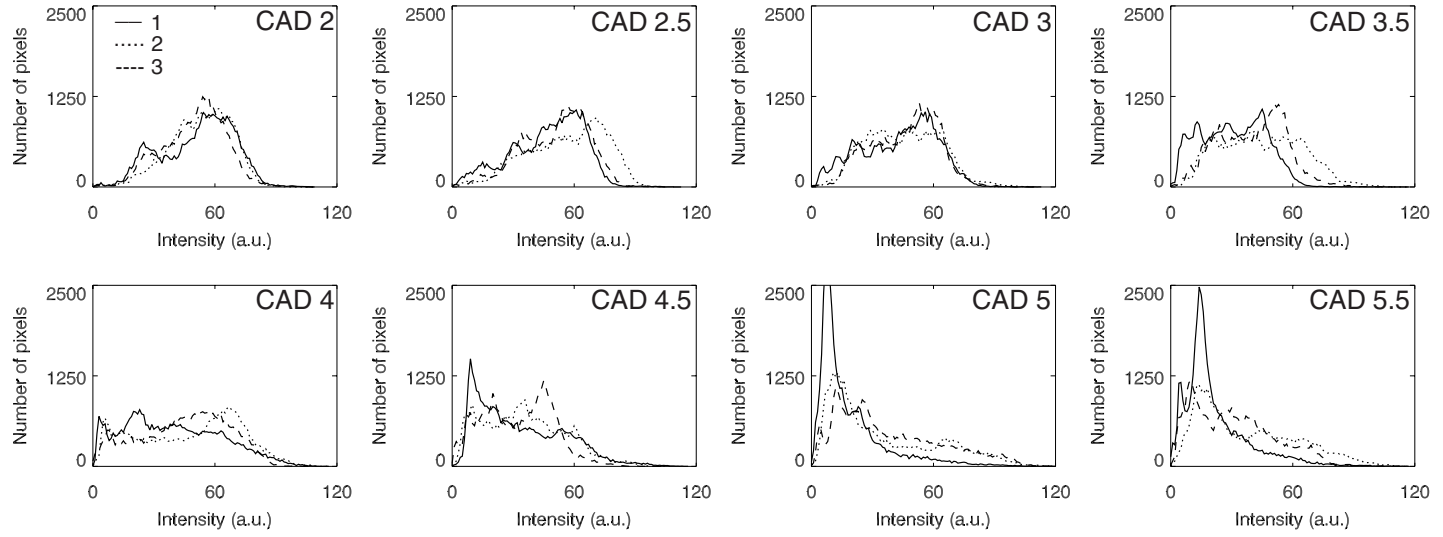

Figure 10: HCCI fuel concentration histograms, calculated from the PLIF examples no:1-3.

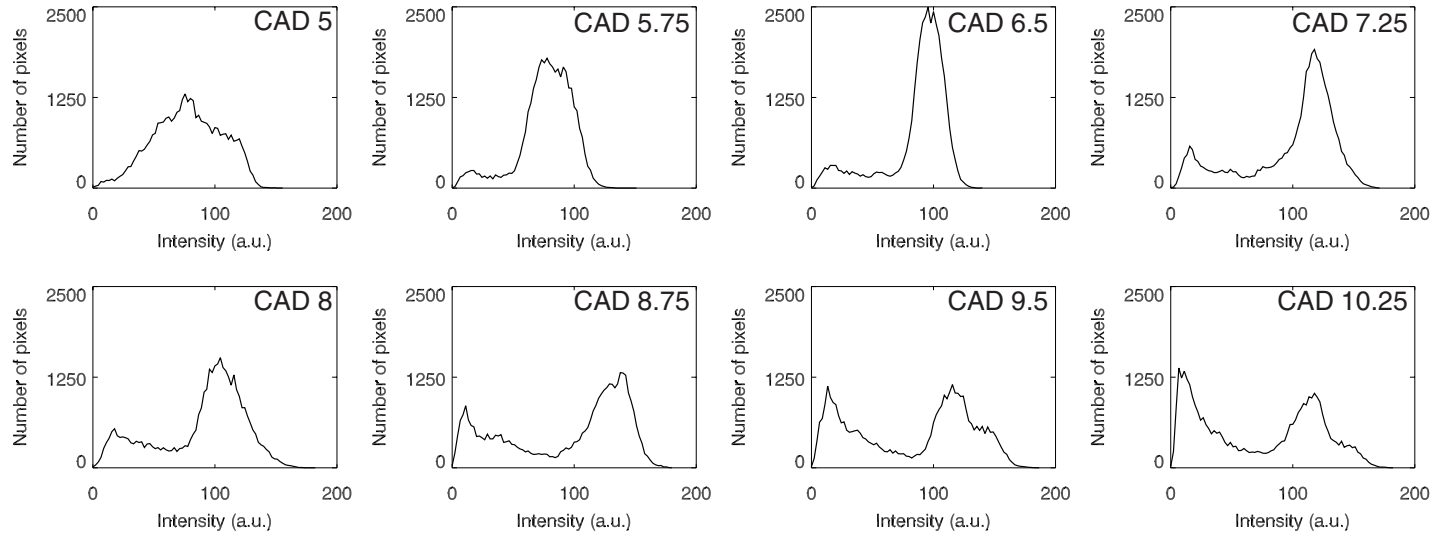

Figure 11: SI fuel concentration histograms, calculated from the corresponding sequence (Figure 9).

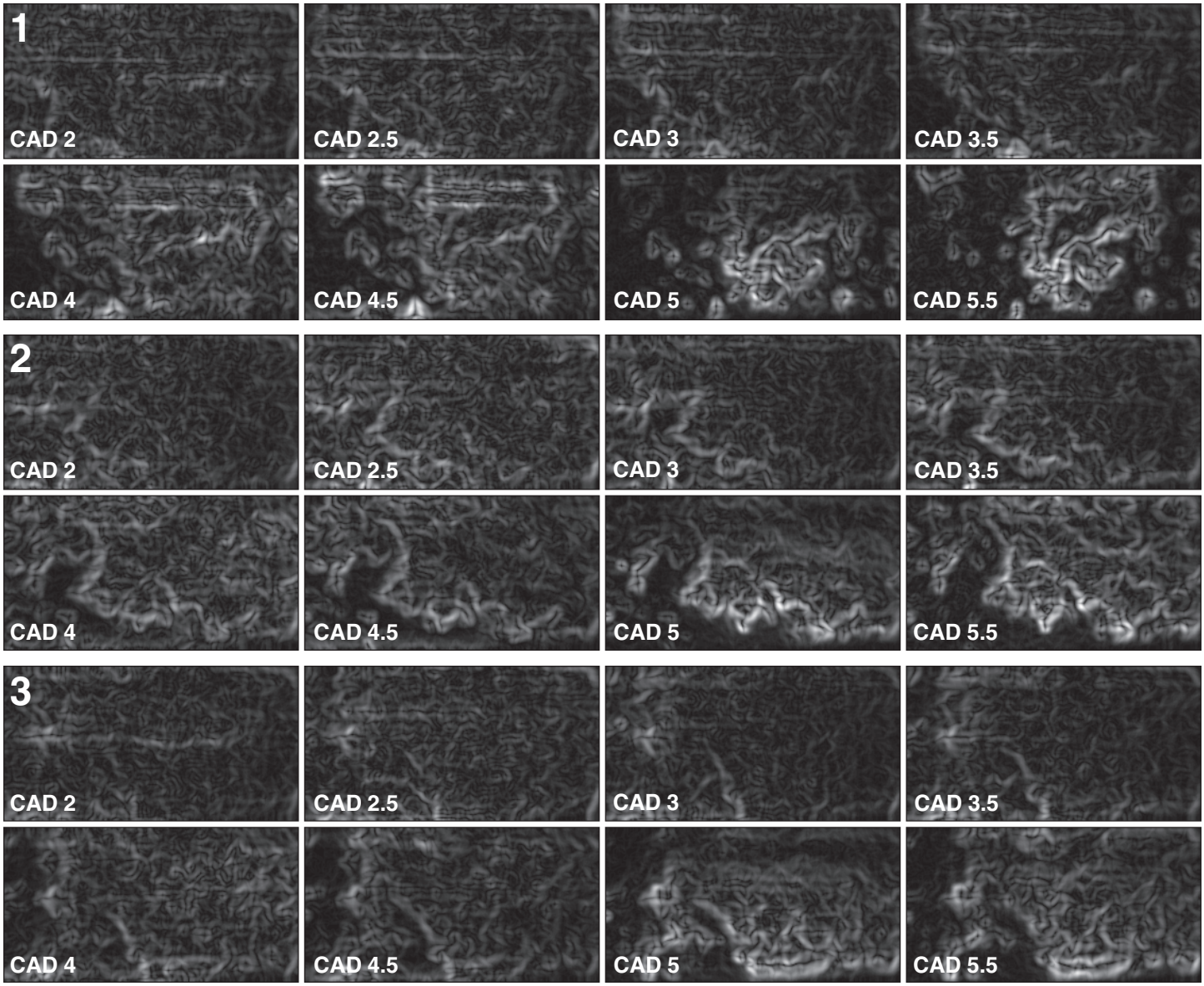

Figure 12: Gradient fields calculated from HCCI sequences no: 1-3 in Figure 8.

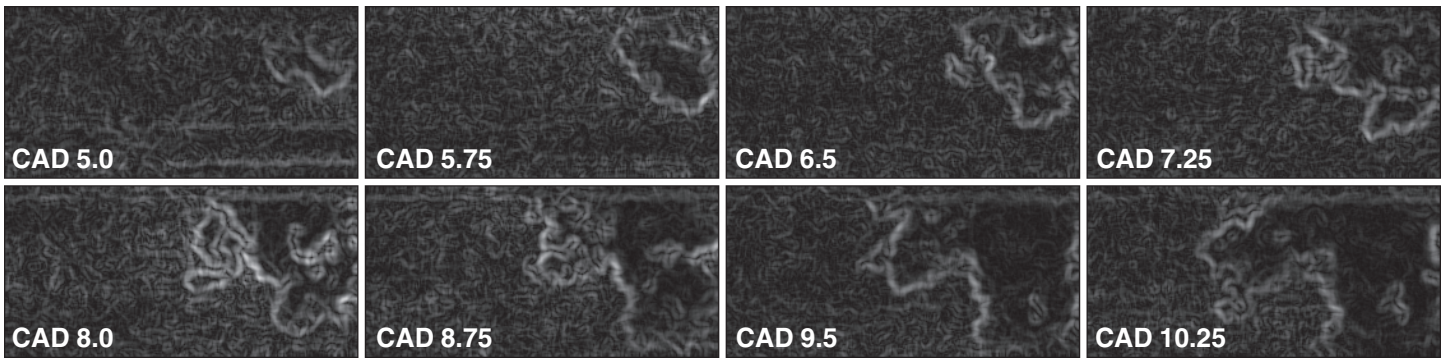

Figure 13: Gradient fields calculated from the SI sequence in Figure 9.

In the later part of the HCCI combustion process, sharp borders between fuel and burnt gases are found in some regions, a phenomenon resembling SI combustion. These sharp borders can either be associated with propagating flame fronts or compression of unburned regions due to the expansion of burnt gases. However, even this late in the fuel consumption process there are still regions of gradually decreasing fuel concentrations, without sharp gradients.

To further explore the fuel consumption process in the HCCI engine, examples of fuel concentration distributions and concentration gradient distributions in HCCI and SI engines are presented. Intensity histograms corresponding to the images in Figure 8 are shown in Figure 10, where fuel

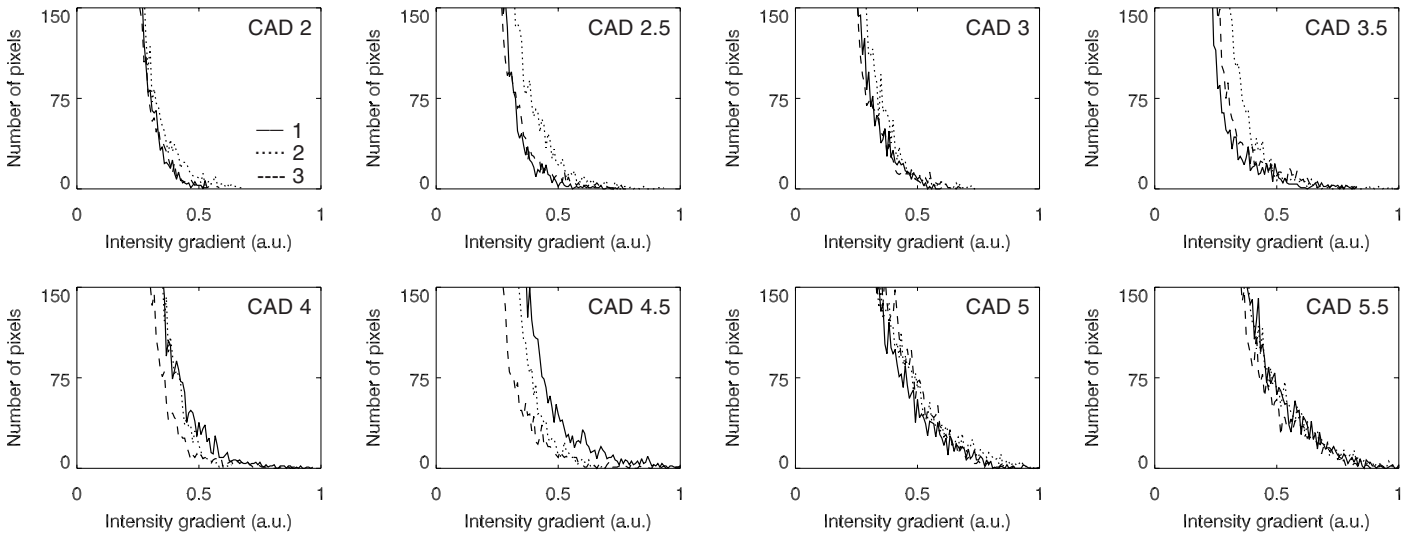

Figure 14: Histograms of fuel concentration gradient fields in HCCI combustion, no:1-3 in Figure 12.

concentration histograms for the three sequences are plotted together for each crank angle position. In the beginning of the combustion process, the fuel concentration distribution is centered around an intensity of 55 counts. The width of the distribution is dependent on the commencing fuel consumption, but also on experimental factors. Non-perfect compensations for beam profile inhomogeneities and laser sheet absorption both lead to a broadening of the ideally narrow distribution, which would correspond to a homogeneous fuel concentration. As the combustion consumes more and more fuel, the fuel concentration distribution gradually shifts to lower concentrations, and at the end of the combustion it peaks close to zero, which corresponds to burnt gases.

If the fuel mixture was to burn as a propagating flame, two distinct peaks, corresponding to burnt and unburned gases, would be visible in the HCCI fuel concentration distribution at intermediate points in time, 4-4.5 CAD. In Figure 11, the fuel concentration distribution corresponding to the SI combustion in Figure 9 is shown as a comparison. Here, two distinct peaks are found at intermediate points in time in the combustion process. In the HCCI case only two very weak and blurred peaks can be found at these times, which indicates that there is no flame propagation. Instead, the distribution slowly shifts from high to low values, as fuel is consumed at different rates in different regions.

In Figure 12, the gradients of Figure 8 are shown. Strong gradients indicate sharp borders between areas of high and low fuel concentrations. At the beginning of the combustion there are not many strong gradients. These appear later, around 3-5 CAD, and the strongest gradients are found at the end of the combustion process. For comparison, the gradient images calculated from the SI combustion in Figure 9 are shown in Figure 13. In the HCCI fuel concentration fields, strong gradients are spread over a larger part of the imaged area than in the SI case, as there is more structure in the HCCI fuel distribution after the onset of combustion. In Figure 14, the distribution of gradients in the HCCI fuel concentration images is shown. Since we are interested in the strong gradients, the histograms have been scaled to show these and not the dominating low gradient peak, which corresponds to the large dark regions in Figure 12. The sharpening of borders between high and low fuel concentration during the HCCI combustion process is clearly seen in these histogram series, as the number of high gradients (gradient intensity >0.5 in Figure 14) increase with time.

However, as mentioned above this does not automatically imply that propagating flames are present during the later stages of HCCI combustion. The underlying cause for the increase in strong gradients can also be compression of the fuel structures by hot product gases.

COMBUSTION RATE ESTIMATION

Figure 16 and Figure 18 show two additional example sequences on how the HCCI combustion process progresses from the start of combustion until 50-60% of the fuel is burned, see Figure 15. From these images it is clear that ignition occurs in many places simultaneously and that the early combustion consists of gradual conversion of fuel. As the combustion progresses, the gradients between combustion products and unburned fuel increase and the combustion process exhibits a behavior similar to flame propagation in SI engines. Thus the question is whether or not this behavior is flame propagation in the sense usually discussed in the context of turbulent flames in engines. The ordinary definition of a premixed flame is a self-sustainable flame front that propagates through an air/fuel mixture, leaving only combustion products behind. However, the HCCI is normally run outside the regular flammability limits comprising very lean mixtures, which at normal conditions do not allow a self-sustained flame. Of key importance and a complicating circumstance is of course, in premixed flames, the turbulence. The turbulence enhances flame speed because of the enlargement of the flame area and the improved mixing. At an extreme level of turbulence, the mixing can be too intense, causing quenching of the flame. Under favorable conditions, the turbulent flame

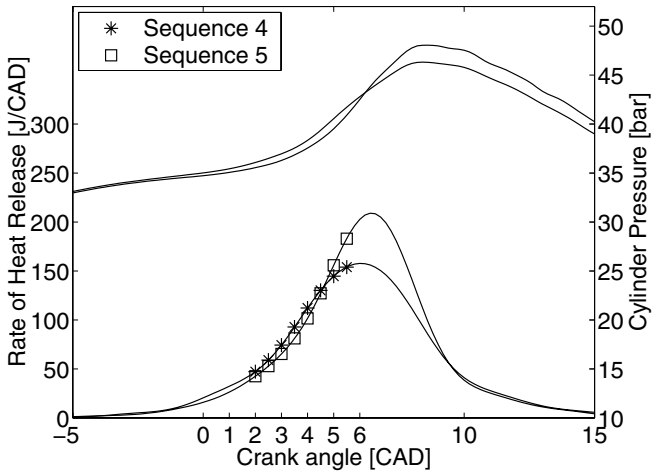

Figure 15: Pressure trace and rate of heat release, no: 4-5.

speed can be several times the laminar flame speed. The turbulent flame speed is often used to characterize a turbulent flame. In the case of HCCI, an estimate of how fast the structures of the HCCI combustion process are growing can indicate if flame propagation is a plausible mechanism.

To estimate the reaction front spreading velocity, the fuel tracer PLIF images were thresholded to separate burned and unburned areas with distinct borders. Figure 17 and Figure 19 show the result of the threshold operation on the corresponding PLIF sequence. From the figures, it is clear that the thresholded PLIF data agrees well with the original set of data. In the images, the charge seems to have a preference to burn from left to right, and by assuming a fictitious, even, reaction front, burning the charge from left to right, a spreading velocity (Vs) can be obtained.

$$Vs = - dA/dt * 1/lf \qquad (2)$$

This estimate is based on a reaction front length (lf) and the rate of burned area growth (dA/dt). If an estimate analogous with turbulent flame propagation is desired, the reaction front length can be the same as the height of the images; lf=42 mm. From Figure 20 and Figure 21 the expansion rate of the burned areas can be estimated to dA/dt=3.45 m^2/s. With these figures, the resulting spreading velocity would be about 82 m/s. A spreading velocity that high is not very common in turbulent flames and it is probable that either the reaction front length is grossly underestimated, or that the mechanism driving the spreading velocity has nothing in common with turbulent flame propagation. For reference, the expansion rate of burned area is about 0.65 m^2/s in the SI combustion case discussed above.

The apparently very high propagation speed shows that, on a global scale, normal flame propagation is highly unlikely. Instead, the combustion onset to the left in the images will enhance a pressure driven temperature increase in the entire combustion chamber, thereby

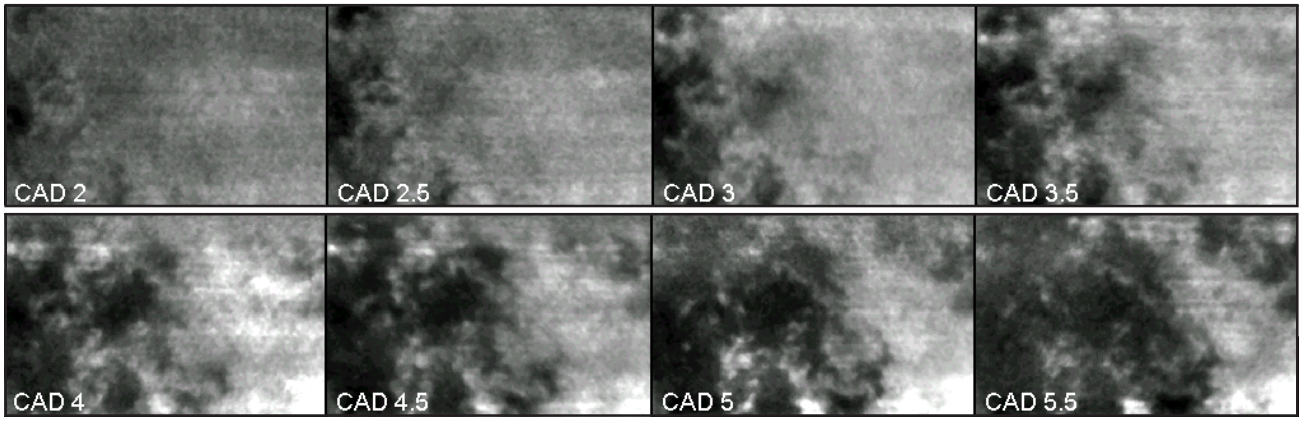

Figure 16: PLIF sequence no: 4 on HCCI combustion.

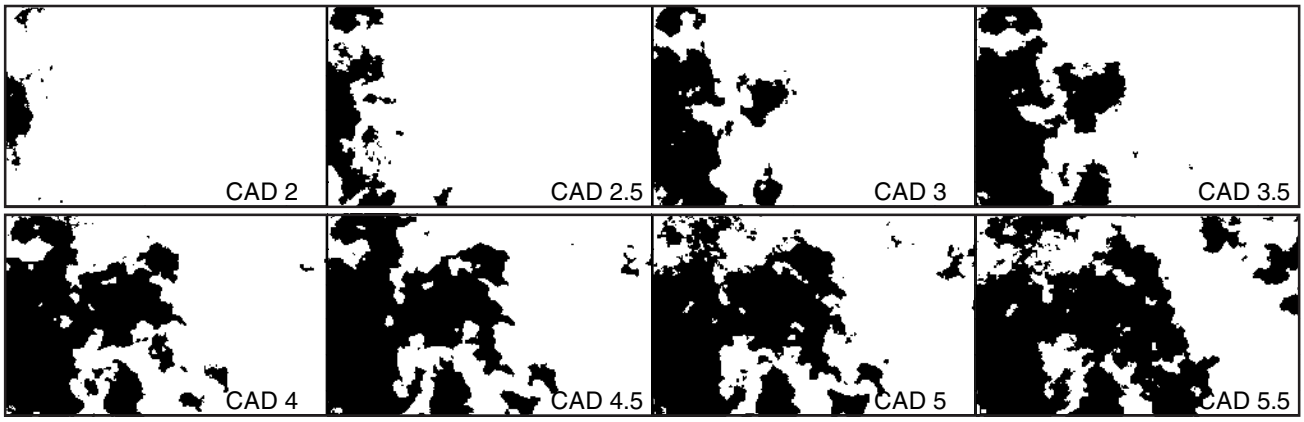

Figure 17: Thresholded data calculated from example sequence no: 4.

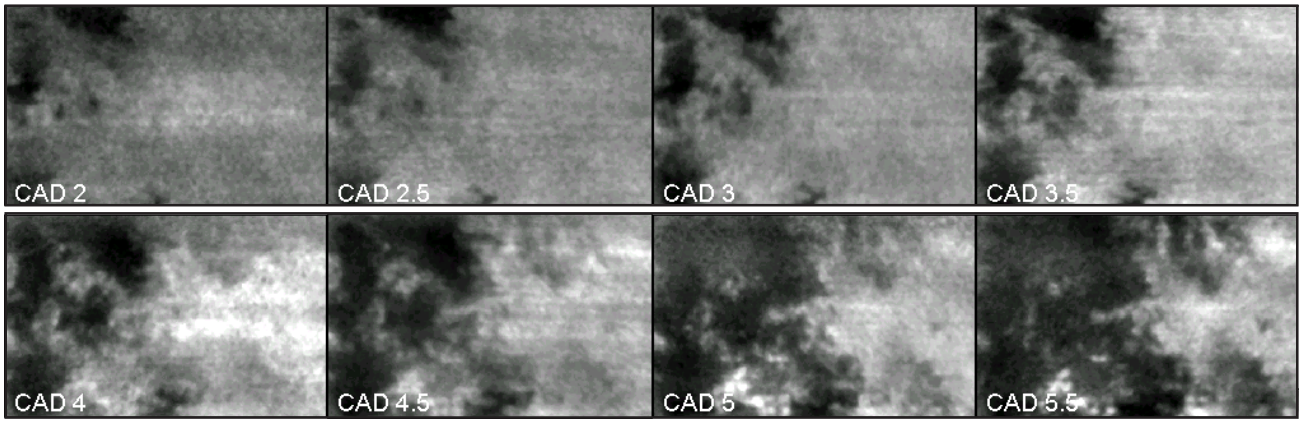

Figure 18: PLIF sequence no:5 on HCCI combustion.

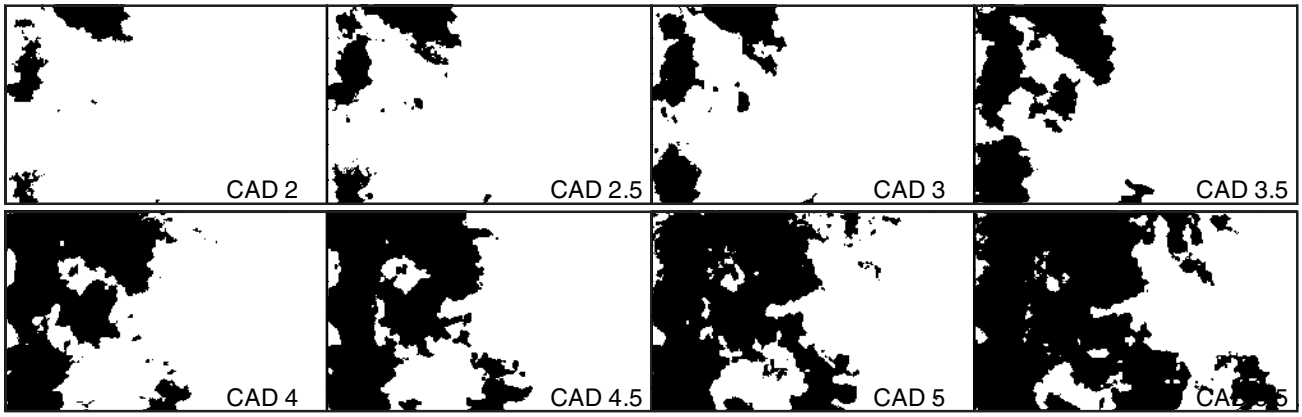

Figure 19: Thresholded data calculated from example sequence no: 5.

generating more favorable conditions for fuel oxidization in the zone to the right.

If the structures are studied on a more detailed level instead, targeting the growths of small islands of burnt areas, their reaction fronts are found to be spreading with velocities in the range of 5-30 m/s, with an average of approximately 15 m/s. Such an expansion speed is in the same range as the turbulent expansion speed found in SI engines. This can then be interpreted as a local propagation of the reaction zone in a fashion similar to that of turbulent flames. However, the measurement data used for this analysis represent growth of small islands of burned charge in a thin sheet. The real combustion process is highly 3-dimensional. This means that the apparent island growth in the plane of measurement could be part of a more complex growth in three dimensions. It would thus be preferable to have the 3D instead of the 2D structure to draw any certain conclusions.

An interesting comparison can be made with a recent work by Schiessl et. al. where the expansion velocities of hot-spots in the end-gas of a knocking SI-engine were investigated. Those experiments concluded an average expansion velocity of 25m/s with a standard deviation of 16 m/s [27].

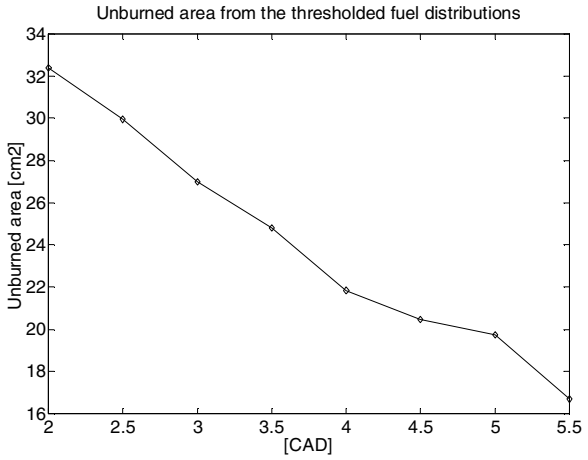

Figure 20: Unburned area from example no: 4, Figure 17.

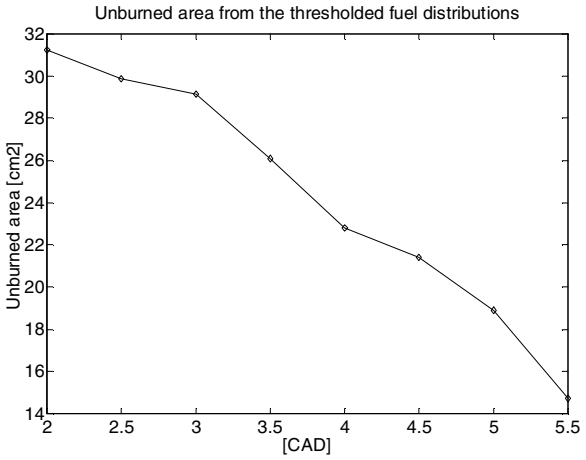

Figure 21: Unburned area from example no: 5, Figure 19.

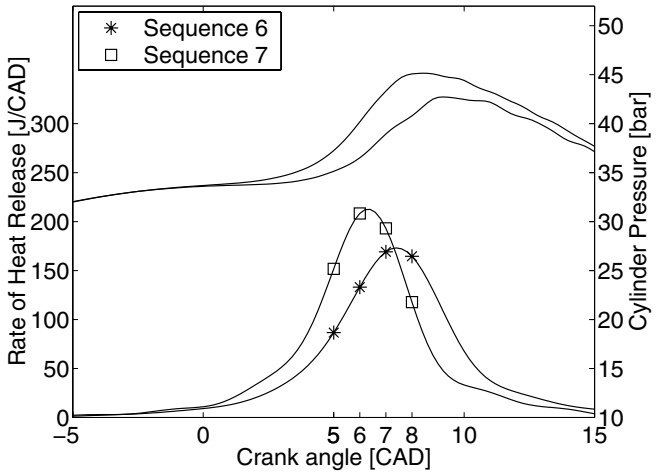

Figure 22: Pressure trace and rate of heat release, no: 6-7.

SIMULTANEOUS PLIF AND CHEMILUMINESCENCE IMAGING

Figure 23 and Figure 24 are examples of simultaneously recorded PLIF and chemiluminescence sequences. The corresponding pressure traces are shown in Figure 22. As outlined above, the PLIF sequence has been normalized. From the chemiluminescence sequence, only the background has been subtracted. In the images, bright areas correspond to high concentrations of fuel and high chemiluminescence intensities respectively. In prior experiments [18], the chemiluminescence intensity was found to correlate very well with the rate of heat release. Thus, a locally high chemiluminescence intensity means that locally, there is a high rate of fuel conversion.

Combustion has just started in the first frame of Figure 23. The PLIF image at 5 CAD indicates that fuel has been consumed in the lower right corner. At the same time the chemiluminescence image shows activity in both the lower right and the lower left corner. This discrepancy could be an effect of chemiluminescence imaging being a line of sight integration. The chemiluminescence is integrated through the 9-10 mm high combustion chamber, whereas PLIF visualizes a thin slice of the combustion chamber. However, it could also be an evidence of gradual fuel decomposition at different stages in space and time. At 6 CAD, some fuel has been gradually consumed in the lower left corner and at the same time the chemiluminescence image indicates increased activity in the same area. The burned region in the lower right corner seems to have expanded a bit. At 7-8 CAD the PLIF image indicates a pocket of unburned fuel in the center that is compressed by the burned gases. Concurrently, the chemiluminescence images show that increasing reaction activity is approaching the pocket of unburned fuel. At this time, the bright features in the PLIF image match the dark features in the chemiluminescence image very well.

The second example sequence, Figure 24, shows a similarly good match between PLIF and chemiluminescence. The combustion process has gradually consumed fuel in the lower part of the images at 5-6 CAD. As the combustion progresses, the structures of unburned fuel become more pronounced and the

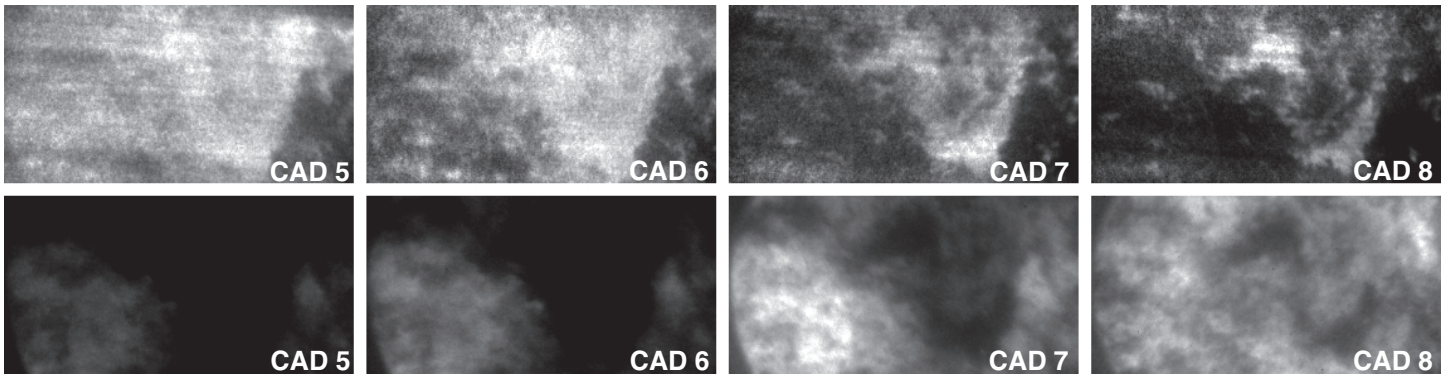

Figure 23: Sequence of simultaneously recorded fuel tracer PLIF (upper row) and chemiluminescence light (lower row) in the HCCI engine, sequence no: 6.

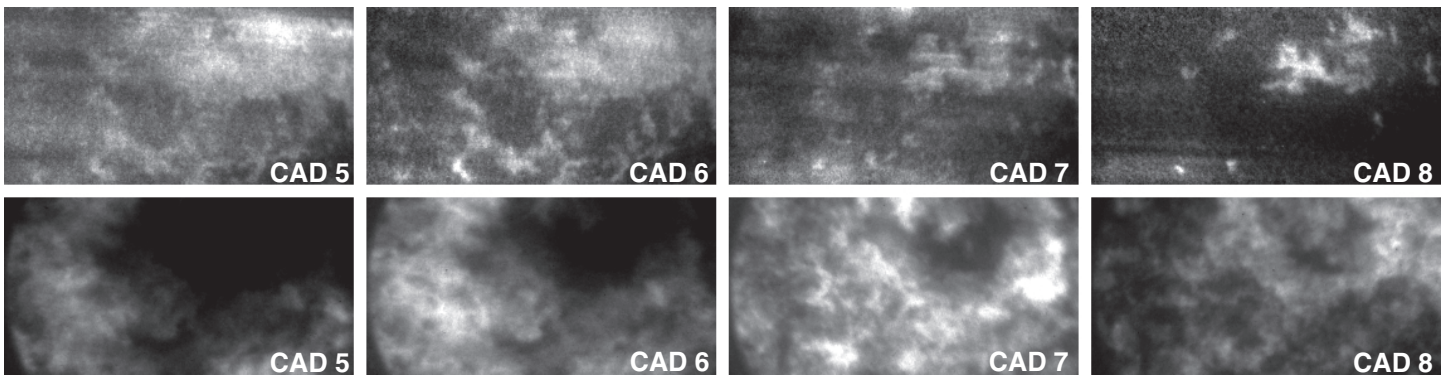

Figure 24: Sequence of simultaneously recorded fuel tracer PLIF (upper row) and chemiluminescence light (lower row) in the HCCI engine, sequence no: 7.

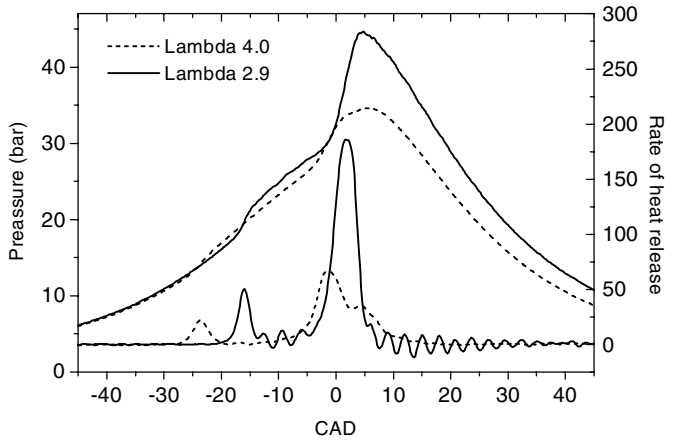

Figure 25: Pressure trace and rate of heat release for λ=4.0 and λ=2.9 during HCCI combustion in the Volvo TD-100 engine.

combustion process exhibits a behavior similar to flame propagation in SI engines. The areas of burned gases grow with rather steep gradients between the burned and the unburned gases. From these findings with simultaneous imaging of fuel concentration and chemiluminescence it is concluded that acetone is an appropriate marker of burned, gradually burned and unburned zones in HCCI.

AIR FUEL VARIATION

To investigate the influence of stoichiometry on the ignition and combustion events, tests were carried out in the TD100 optical engine. Two cases with different lambda values were evaluated, one with lean combustion at lambda 4.0 and another, slightly richer, at lambda 2.9. The rich limit was governed by the rate of pressure rise and peak-pressure. For fuel, a blend of n-heptane (75%) and acetone (25%) was used.

In Figure 25, the pressure trace and rate of heat release are displayed. As expected, the heat release calculated from the pressure data revealed a much faster combustion for the richer mixture. Due to the occurrence of early cool-flames when using n-heptane, the conventional 5-95% burnt mass is not a good interval for defining the combustion duration. Instead, 20-90% was used for these measurements. For the lean case (lambda=4.0) the calculated combustion duration was approximately 12 cad. For the richer case (lambda=2.9) the corresponding value was about 6 cad. These readings are well supported by the results from the PLIF measurements, which are shown in Figure 26 and Figure 27.

In terms of ignition behavior and spatial structure of the combustion, the two cases showed similar results. Also, no distinct difference regarding the combustion process in the optical Scania engine were found. This means that a horizontal as well as a vertical laser sheet in two different engines produce the same results. With this in mind, the conclusions ought not to be entirely based on a specific laser sheet or engine configuration.

SUMMARY AND CONCLUSIONS

- A unique high-speed laser and camera system was used to visualize the HCCI combustion process. During a single cycle, eight individual laser pulses were captured on eight ICCD cameras.
- A good correlation between the consumption of fuel tracer and chemiluminescence intensity confirmed that fuel tracer PLIF is suitable for studying the combustion process.
- The PLIF sequences showed that during the first stage of combustion, a well-distributed gradual decay of fuel concentration occurs.
- During the later parts of the combustion process, the fuel concentration images present much more structure, with distinct edges between islands of unburned fuel and products.
- The transition from the evenly distributed fuel oxidation in the beginning to the large structures at the end is most likely the result of a gradual amplification of small temperature inhomogeneities and the expansion of

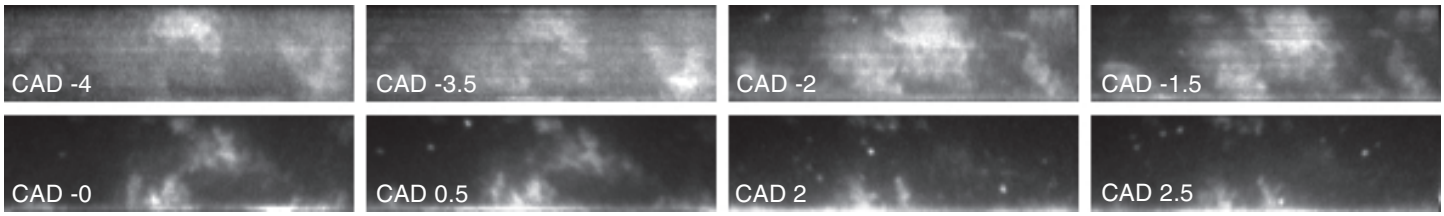

Figure 26: PLIF sequence no: 8 at λ=4.0, from the Volvo TD-100.

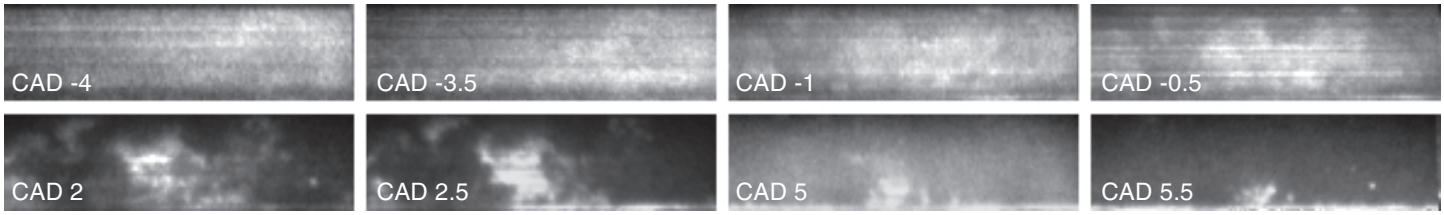

Figure 27: PLIF sequence no: 9 at λ=2.9, from the Volvo TD-100.

burned gas compressing the unburned. If the combustion is only slightly faster in one location, the temperature will increase, thus making the chemical reactions faster, which in turn will increase the temperature and so on.

- Image processing was performed to generate intensity histograms. This revealed that the transition from fuel to products in the HCCI engine was a gradual process. With a wide distribution of intensity (fuel concentration), close to 50% burned. This was in contrast to the results for an SI engine. The SI engine intensity histogram showed basically two peaks, one for unburned fuel and one for burned.

- Threshold image processing, generating binary images, made it possible to estimate an area expansion speed, both globally and locally.

- The resulting global propagation speed was found to be 82 m/s. This is much higher that any deflagration speed found in an SI engine. Thus it can be concluded that the HCCI combustion process does not take place through flame propagation.

- Evaluation of small island growth showed that the local combustion zone expanded with a speed on the order of 15 m/s. This is similar to the turbulent flame propagation speed normally found in SI engines.

- The engine configuration, laser sheet orientation and air/fuel ratio did not influence the general results presented.

- Three combustion modes were observed in the HCCI combustion process:

    1. The initial combustion onset, which is very evenly distributed, with no flame propagation present.

    2. Increased chemical activity. As the chemical reactions start, the heat generated will increase temperature. Any minor variation in temperature or other distribution affecting chemical reaction speed will be amplified due to positive feedback. At the most favorable positions kernels are formed. The number and locations of kernels are dependent on global parameters like distribution of air, fuel, inert gas and temperature. The initial ignition kernels grow larger as combustion progresses.

    3. The forming of new ignition kernels. At locations with favorable conditions, new ignition kernels form during the combustion progress due to the increased temperature. These new kernels grow until they merge with others.

ACKNOWLEDGMENTS

The authors would like to extend their gratitude to Mr. Greger Juhlin at Scania CV AB and “Programrådet för Fordonsteknisk Forskning” (PFF) for sponsoring part of this investigation. Financial support was also supplied by CECOST and the Swedish Research council. We would also like to thank the HCCI engine consortium in Lund. Thanks also to Mr. Bertil Andersson and Mr. Jan-Erik Nilsson for their invaluable assistance and maintenance of the experimental apparatus. All of this work was conducted at the Lund Institute of Technology in Sweden.

REFERENCES

1. S. Onishi, S. Hong Jo, K. Shoda, P. Do Jo, S. Kato: “Active Thermo-Atmosphere Combustion (ATAC) - A New Combustion Process for Internal Combustion Engines”, SAE790501.
2. R.H. Thring: “Homogeneous-Charge Compression-Ignition (HCCI) Engines”, SAE892068.
3. A. Hultqvist, M. Christensen, B. Johansson, A. Franke, M. Richter, M. Aldén: “A Study of the Homogeneous Charge Compression Ignition Combustion Process by Chemiluminescence Imaging”, SAE1999-01-3680.
4. M. Christensen, B. Johansson: “Influence of Mixture Quality on Homogeneous Charge Compression Ignition”, SAE9824541.
5. T. Aoyama, Y. Hattori, J. Mizuta, Y. Sato: ”An Experimental Study on a Premixed-Charge Compression Ignition Gasoline Engine”, SAE960081.
6. J-O. Olsson, O. Erlandsson, B. Johansson: “Experiments and Simulation of a Six-Cylinder Homogeneous Charge Compression Ignition (HCCI) Engine”, SAE2000-01-2867.
7. M. Christensen, A. Hultqvist, B. Johansson: “Demonstrating the Multi Fuel Capability of a Homogeneous Charge Compression Ignition Engine with Variable Compression Ratio”, SAE1999-01-3679.
8. M. Christensen, P. Einewall, B. Johansson: “Homogeneous Charge Compression Ignition (HCCI) Using Iso-octane, Ethanol and Natural Gas- A Comparison to Spark Ignition Operation”, SAE972874.
9. J-O. Olsson, P. Tunestal, B. Johansson: ” Closed-Loop Control of an HCCI Engine”, SAE2001-01-1031.
10. J-O. Olsson, P. Tunestal, G. Haraldsson, B. Johansson: “A Turbo Charged Dual Fuel HCCI Engine”, SAE2001-01-1896.
11. O. Erlandsson, B. Johansson, F. A. Silversand: “Hydrocarbon (HC) Reduction of Exhaust Gases from a Homogeneous Charge Compression Ignition (HCCI) Engine Using Different Catalytic Mesh-Coatings”, SAE2000-01-1847.
12. D. Law, J. Allen, D. Kemp, G. Kirkpatrick, T. Copland: “Controlled Combustion in an IC-Engine with a Fully Variable Valve Train”, SAE2001-010251.

13. M. Richter, A. Franke, M. Aldén, A. Hultqvist, B. Johansson: ‘‘Optical Diagnostics Applied to a Naturally Aspirated Homogeneous Charge Compression Ignition Engine”, SAE1999-01-3649.
14. M. Richter, J. Engström, A. Franke, M. Aldén, A. Hultqvist, B. Johansson: ‘‘The influence of charge inhomogeneity on the HCCI combustion process”, SAE2000-01-2868.
15. H. Akagawa, T. Miyamoto, A. Harada, S. Sasaki, N. Shimazaki, T. Hashizume, K. Tsujimura: ‘‘Appraoches to solve problems of the premixed lean diesel combustion”, SAE1999-01-0183.
16. Y. Iwabuchi, K. Kawai, T. Shoji, Y. Takeda: ‘‘Trial of a New Concept Diesel Combustion System - Premixed Compression-Ignited Combustion”, SAE1999-01-0185.
17. G. Andrews, K. Zaidi: ‘‘Partial Premixed Diesel Gaseous and Particulate Emissions”, SAE1999-01-0838.
18. A. Hultqvist, M. Christensen, B. Johansson, A. Franke, M. Richter, M. Aldén: ‘‘A Study of the Homogeneous Charge Compression Ignition Combustion Process by Chemiluminescence Imaging”, SAE1999-01-3680.
19. A. Hultqvist, U. Engdar, B. Johansson, J. Klingmann: “Reacting Boundary Layers in a Homogeneous Charge Compression Ignition (HCCI) Engine”, SAE2001-01-1032.
20. B.Yip, M. F. Miller, A. Lozano, R. K. Hanson: “A combined OH/acetone planar laser-induced fluorescence imaging technique for visualizing combusting flows”, Experiments in Fluids, Vol. **17**, 1994, pp 330-336.
21. F. Grossmann, P. B. Monkhouse, M. Ridder, V. Sick, J. Wolfrum: “Temperature and pressure dependence of the laser induced fluorescence of gas-phase acetone and 3-pentanone”, Appl. Phys. B, Vol. **62**, 1996, pp 249-253.
22. F. Grossmann, P. B. Monkhouse, M. Riddler, M. C. Thurber, F. Grisch, B. J. Kirby, M. Votsmeier, R. K. Hanson: “Measurements and modeling of acetone laser-induced fluorescence with implications for temperature-imaging diagnostics”, App. Opt., Vol. **37**, No. 21, 1998, pp 4963-4978.
23. J. Nygren, M. Richter, J. Hult, C. F. Kaminski, M. Aldén: “Temporally resolved single cycle measurements of fuel- and OH-distributions in a spark ignition engine using high speed laser spectroscopy”, Proceedings of The Fifth International Symposium on Diagnostics and Modeling of Combustion in Internal Combustion Engines (COMODIA), July 2001, Nagoya, Japan, pp 572-580.
24. M. Sonka, V. Hlavac, R. Boyle: Image Processing, Analysis and Machine Vision, (Chapman&Hall, London, 1993), pp 61-67.
25. C.F. Kaminski, J. Hult, and M. Aldén, “High repetition rate planar laser induced fluorescence of OH in a turbulent non-premixed flame”, Appl. Phys. B, Vol. **68**, 1999, pp 757-760.
26. M. C. Thurber, R. K. Hanson: “Pressure and composition dependence of acetone laser-induced fluorescence with excitation at 248, 266 and 308 nm”, Appl. Phys. B, Vol. **69**, 1999, pp 229-240.
27. R. Schiessl, A. Dreizler, U. Maas, A. J. Grant, P. Ewart: “Double-Pulse PLIF Imaging of Self-Ignition Centers in an SI Engine”, SAE2001-01-1925.

CONTACT

Corresponding author:
Anders Hultqvist

Address:
Lund Institute of Technology
Dept. of Heat and Power Engineering
Division of Combustion Engines
P.O. Box 118
S-221 00, Lund
Sweden

E-mail:
anders.hultqvist@vok.lth.se